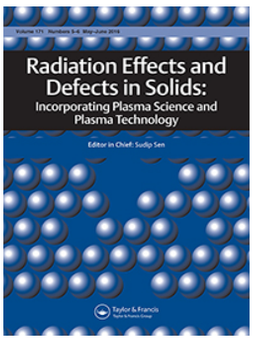

Taylor & Francis
Taylor & Francis Group

Radiation Effects and Defects in Solids

Incorporating Plasma Science and Plasma Technology

ISSN: 1042-0150 (Print) 1029-4953 (Online) Journal homepage: http://www.tandfonline.com/loi/grad20

Effect of 100 MeV swift Si^{8+} ions on structural and thermoluminescence properties of $Y_2O_3:Dy^{3+}$nanophosphor

N. J. Shivaramu, B. N. Lakshminarasappa, K. R. Nagabhushana & Fouran Singh

To cite this article: N. J. Shivaramu, B. N. Lakshminarasappa, K. R. Nagabhushana & Fouran Singh (2016) Effect of 100 MeV swift Si^{8+} ions on structural and thermoluminescence properties of $Y_2O_3:Dy^{3+}$nanophosphor, Radiation Effects and Defects in Solids, 171:5-6, 408-420, DOI: 10.1080/10420150.2016.1194419

To link to this article: http://dx.doi.org/10.1080/10420150.2016.1194419

Published online: 08 Jun 2016.

RADIATION EFFECTS & DEFECTS IN SOLIDS, 2016
VOL. 171, NOS. 5–6, 408–420
http://dx.doi.org/10.1080/10420150.2016.1194419

Taylor & Francis
Taylor & Francis Group

Effect of 100 MeV swift Si^{8+} ions on structural and thermoluminescence properties of Y_2O_3:Dy^{3+} nanophosphor

N. J. Shivaramu[a,b], B. N. Lakshminarasappa[b], K. R. Nagabhushana[c] and Fouran Singh[d]

[a]Department of Physics, Indian Academy Degree College, Bangalore, India; [b]Department of Physics, Bangalore University, Bangalore, India; [c]Department of Physics (S & H), PES University, Bangalore, India; [d]Inter University Accelerator Centre, New Delhi, India

ABSTRACT

Nanoparticles of Y_2O_3:Dy^{3+} were prepared by the solution combustion method. The X-ray diffraction pattern of the 900°C annealed sample shows a cubic structure and the average crystallite size was found to be 31.49 nm. The field emission scanning electron microscopy image of the 900°C annealed sample shows well-separated spherical shape particles and the average particle size is found to be in a range 40 nm. Pellets of Y_2O_3:Dy^{3+} were irradiated with 100 MeV swift Si^{8+} ions for the fluence range of 3×10^{11}–3×10^{13} ions cm^{-2}. Pristine Y_2O_3:Dy^{3+} shows seven Raman modes with peaks at 129, 160, 330, 376, 434, 467 and 590 cm^{-1}. The intensity of these modes decreases with an increase in ion fluence. A well-resolved thermoluminescence glow with peaks at $\sim$414 K (T_{m1}) and $\sim$614 K (T_{m2}) were observed in Si^{8+} ion-irradiated samples. It is found that glow peak intensity at 414 K increases with an increase in the dopant concentration up to 0.6 mol% and then decreases with an increase in dopant concentration. The high-temperature glow peak (614 K) intensity linearly increases with an increase in ion fluence. The broad TL glow curves were deconvoluted using the glow curve deconvoluted method and kinetic parameters were calculated using the general order kinetic equation.

ARTICLE HISTORY
Received 2 December 2015
Accepted 16 May 2016

KEYWORDS
XRD; swift heavy ions; Raman spectroscopy; thermoluminescence

PACS
61.05.cp; 25.70.Ef; 78.30.j; 78.60.Kn

1. Introduction

The Y_2O_3 material attracted researchers due to its superior properties such as high melting point (2673 K), low thermal conductivity (33 Wm^{-1} K^{-1}), high thermal stability, wide transparency range (0.2–8 μm) with a large band gap of 5.7 eV, high refractive index (1.8) and low phonon energy (380 cm^{-1}) (*1*, *2*). Y_2O_3 is one of the best hosts for rare-earth (RE) ions, because of similarities in chemical properties and ionic radii of RE ions. Among RE ions, dysprosium (Dy^{3+}) has attracted much attention due to its unique spectral properties, Y^{3+} and Dy^{3+} are trivalent ions having nearly the same ionic radii. Therefore, the Dy^{3+} ion easily substitutes in Y^{3+} sites, which leads to enhancement of optical properties. It is well known that greenish-yellow light can be obtained by mixing blue and yellow light (*3*, *4*). Various techniques are available for the preparation of nanomaterials such as chemical

CONTACT B. N. Lakshminarasappa bnlnarasappa@rediffmail.com

vapor deposition, solid state methods, plasma synthesis, high-energy milling, hydrothermal, sol–gel, spray pyrolysis and co-precipitation methods (*5, 6*). Among these techniques the combustion method is a very easy chemical technique useful for the synthesis of inorganic materials at low temperatures. Furthermore, the technique yields a large surface area and high homogeneity products and allows fine control of the product's chemical composition (*7*).

Raman spectroscopy is one of the non-destructive material characterization technique. Raman spectroscopy is able to deliver structural information on swift heavy ion- (SHI) induced lattice disorder and nature of crystallinity and phonon vibrations because it is sensitive to structural disorder that occurs within optical skin depth of a laser beam (*8*). Thermoluminescence (TL) is a simple technique for investigation of radiation-induced defects. TL and optically stimulated luminescence dosimeters have many advantages over currently used dosimeters in radiotherapy and space dosimetry (*9*) with heavy charged particles. Heavy ion beams have been used for diagnostic and therapeutic purposes (*10*). The treatment with highly energetic ion beams has several advantages in comparison with conventional irradiation with photons. The high-energy particles are present in space environment, where the components used in various subsystems of air crew and space craft get exposed to such radiations. There are several ways of measuring the dose of radiation. At present, the dose of radiation is measured largely using thermoluminescent dosimetry (TLD) badges. There are several materials that exhibit TL properties with ion beam irradiation (*11, 12*). Among these, RE-doped SHI-induced TLD properties have been extensively studied during the past few decades. Dy-doped $CaSO_4$ (*13*) and CaF_2 (*14*) are used for standard dosimetry applications. Sanyal et al. studied the behavior of thermally treated $CaSO_4$:Dy phosphor. The phosphor revealed linear response of the low-temperature glow peak and could be an efficient dosimetry system for the food commodities (*15*). However, efforts are still being made to improve dosimetry for measuring high-energy radiations. The objective of the present work is to study SHI-induced structural modifications and TL properties of Y_2O_3:Dy^{3+} nanophosphor. TL trapping parameters are evaluated by the glow curve deconvoluted (GCD) method and results are discussed in detail.

2. Material and methods

Dy^{3+}-doped yttrium oxide nanophosphor was synthesized by the solution combustion technique, using yttrium nitrate hexahydrate and dysprosium nitrate pentahydrate as oxidizer and urea as fuel. Yttrium nitrate hexahydrate ($Y(NO_3)_3{\cdot}6H_2O$) with 99.8% purity, dysprosium nitrate pent hydrate ($Dy(NO_3)_3{\cdot}5H_2O$) with 99.9% purity were procured from Aldrich Chemicals, urea (CH_4N_2O) with 99.5% purity was procured from Merck Specialties Private Limited. All the chemicals are directly used without any purification. Stoichiometric amount of yttrium nitrate, dysprosium nitrate and urea were dissolved in 50 ml of double distilled water in a cylindrical pyrex dish of 600 ml capacity. The homogeneous mixture was introduced into a muffle furnace maintained at 500 ± 5°C. Initially, the solution boils and undergoes dehydration followed by decomposition with evaporation of a large amount of gases leaving behind the powder. The final product is voluminous and whitish in nature (*11*). The synthesized powder was annealed at 900°C for 2 h (*7, 16*). Pellets of Y_2O_3:Dy^{3+} samples were prepared based on the procedure discussed elsewhere (*16*) and pellets irradiated with 100 MeV swift Si^{8+} ions having 2 pnA current using 15 UD Pelletron at

the Inter University Accelerator Centre, New Delhi, India. The irradiation fluences were varied from 3×10^{11} to 3×10^{13} ions cm^{-2}. Pellets were characterized by the X-ray diffraction (XRD) technique using the Bruker D8 diffractometer, with Cu-K_α radiation of wavelength 1.5406 Å. Morphology of the synthesized samples was studied by field emission scanning electron microscopy (FE-SEM) [MIRA II LMH from TESCAN]. Raman spectra were recorded in the range 100–1000 cm^{-1} using the Renishaw 1000 Raman spectrometer with an excitation wavelength of 514.5 nm from 0.5 mW of Ar ion laser as the excitation source. TL glow curves were recorded at a heating rate of 5 K s^{-1} using the Harshaw TLD reader (Model 3500). All experiments were performed at room temperature.

3. Results and discussion

3.1. X-ray diffraction

Figure 1 shows the XRD patterns of 900°C annealed pristine and 100 MeV swift Si^{8+} ion-irradiated Dy^{3+}- (0.6 mol%) doped Y_2O_3. XRD patterns are indexed to the cubic Y_2O_3 phase with the space group $Ia\bar{3}$ according to the standard card (JCPDS No. 88–1040) (*16, 17*). Further it is observed that ion irradiation does not induce additional peaks and there is no change in peak position. However, peak broadening and decreasing peak intensity are observed after ion irradiation due to loss of crystallinity with an increase in ion fluence. The loss of crystallinity and lattice damage could be interpreted based on the thermal spike model. According to this model, high energy deposited by the ions is diffused to electrons. Then, the electrons transfer their energy to the lattice in solid by electron-atom interaction.

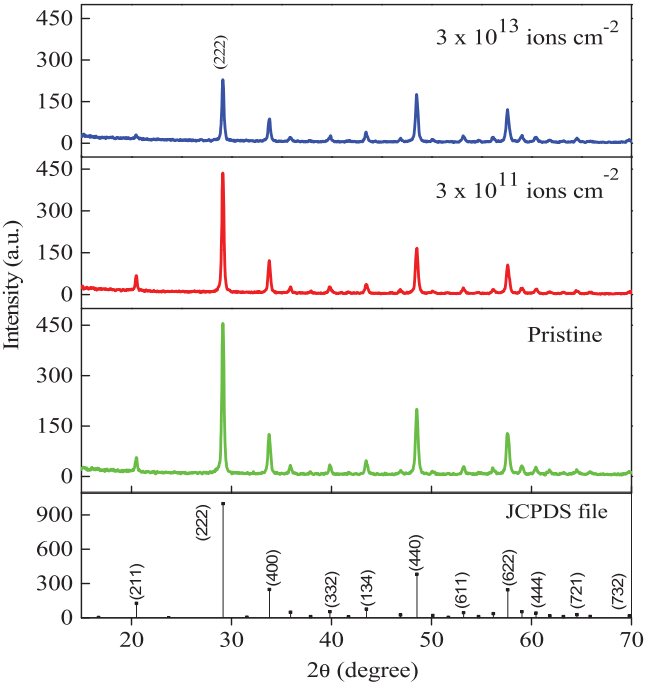

Figure 1. XRD patterns of pristine and SHI-irradiated Dy^{3+} (0.6 mol%) doped Y_2O_3.

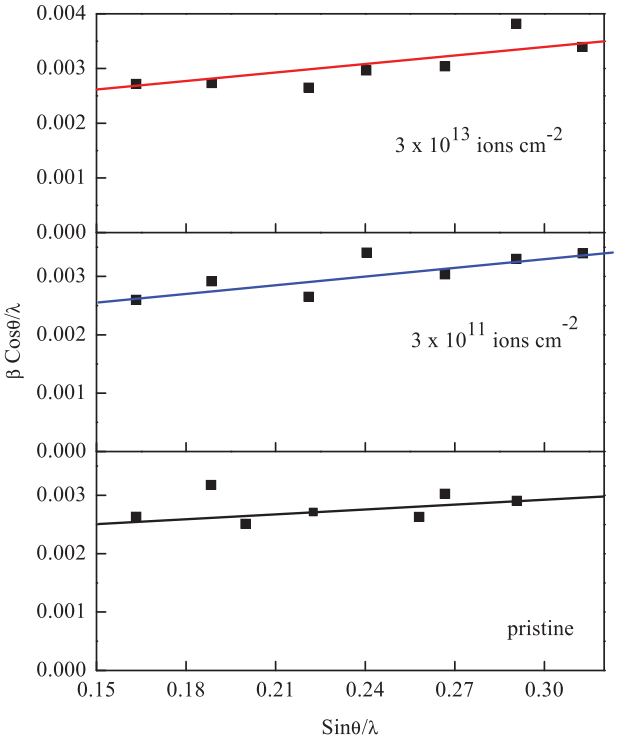

Figure 2. W–H plot of pristine and SHI-irradiated Dy^{3+}-doped Y_2O_3.

Finally, the energy is diffused into lattice and induces a local increase of lattice temperature in the cylindrical ion path region. This local heating followed by a rapid quenching may lead to the loss of crystallinity and lattice disorder (*18*).

The crystallite size and lattice strain are estimated using the Williamson–Hall (W–H) method (*17*, *19*). Figure 2 shows a plot of $\beta \cos\theta/\lambda$ versus $4 \sin\theta/\lambda$. We will get a straight line with a slope equal to the value of the lattice strain and the *y*-axis intercept equal to the inverse of the crystallite size and was found to be 29–36 nm. The average crystallite size of pristine and ion-irradiated samples is also calculated using Scherrer's formula and found to be 20–28 nm. From the XRD data, dislocation density (δ) and the lattice strain are calculated and are found to increase with an increase in ion fluence as shown in Table 1. This is attributed to the ion-induced loss of crystallinity and an increase in lattice disorderness.

Table 1. Structural parameters of pristine and 100 MeV swift Si^{8+}-irradiated Dy^{3+}-doped Y_2O_3.

Ion fluence (ions cm^{-2})	Crystallite size, *D* (nm)		Lattice constant, *a* (Å)	Density, ρ (g cm^{-3})	Dislocation density, δ ($\times 10^{15}$)	Inter-planar space in at (222) (Å)	Lattice strain (%)	
	Scherrer	W–H method					W–H method	Calculated
Pristine	28.10	36.03	10.606	5.028	1.27	3.062	0.065	0.100
3×10^{11}	26.22	34.05	10.609	5.024	1.45	3.063	0.120	0.117
3×10^{13}	20.21	29.00	10.609	5.024	2.44	3.063	0.135	0.170

3.2. FESEM micrograph analysis

FESEM is an important tool for the study of topography and surface morphology of the synthesized nanopowders. It is well known that the combustion synthesized product is highly influenced by fuel to metal–ligand complex formation. Depending on the nature of fuel, fuel to oxidizer ratio, the nature of combustion differs from flaming to non-flaming reactions which involve liberation of enormous amount of gases (*20*). Figure 3(a) shows the FE-SEM image of 900°C annealed Y_2O_3:Dy^{3+} (0.6 mol%) and it is observed that the particles are loosely agglomerated with spherical shape and voids due to the evolution of large amount of gases during the combustion process. And, the average particle size of Y_2O_3:Dy^{3+} is found to be $\sim$22 nm. The composition of the sample is estimated through

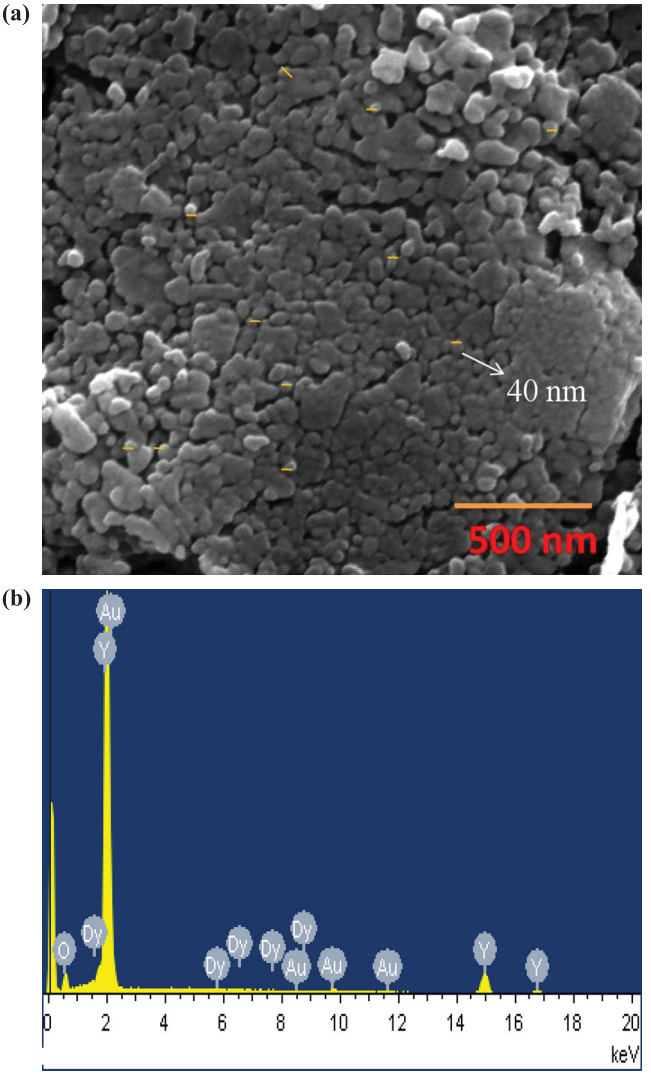

Figure 3. (a) FE-SEM image of 900°C annealed Y_2O_3:Dy^{3+} nanophosphor and (b) EDX of 900°C annealed Y_2O_3:Dy^{3+} nanophosphor.

the energy-dispersive X-ray spectroscopy (EDX) technique. It is proved to be a powerful tool to obtain the elemental composition ratio as shown in Figure 3(b) of the Y_2O_3:Dy^{3+} (0.6 mol%) sample. We can see only the element peaks of Y, O and Dy in the sample. The concentrations of Y, O and Dy in the sample are 32.25, 67.47 and 0.28 at%, respectively.

3.3. Raman spectroscopy

Raman spectroscopy is a very sensitive non-destructive technique and it provides vibration of molecules within the scattering volume. The representation of optical modes in cubic Y_2O_3 are given (*21*) as

$$\Gamma_{op} = 4A_g + 4E_g + 14F_g + 5A_{zu} + 5E_u + 16F_u,$$

where $4A_g$, $4E_g$ and $14F_g$ are Raman active, 16 F_u is IR active and $5A_{zu}$, $5E_u$ are inactive modes. Thus, there are 22 Raman active modes, where E_g and F_g modes are doubly and triply degenerated, respectively. The Raman active modes of cubic Y_2O_3 can be divided into 15 modes ($3A_g + 3E_g + 9F_g$) coming from the vibration of O ions and 7 modes ($A_g + E_g + 5F_g$) coming from the vibration of Y ions (*21*). Figure 4 shows the room temperature Raman spectra of pristine and 100 MeV Si^{8+} ion-irradiated Y_2O_3:Dy^{3+} (0.6 mol%) samples. The Raman modes observed at 129, 330, 376, 434, 467, 590 and 160 cm^{-1} are attributed to F_g and $F_g + A_g$ vibration modes. The Raman active mode of 376 cm^{-1} shows

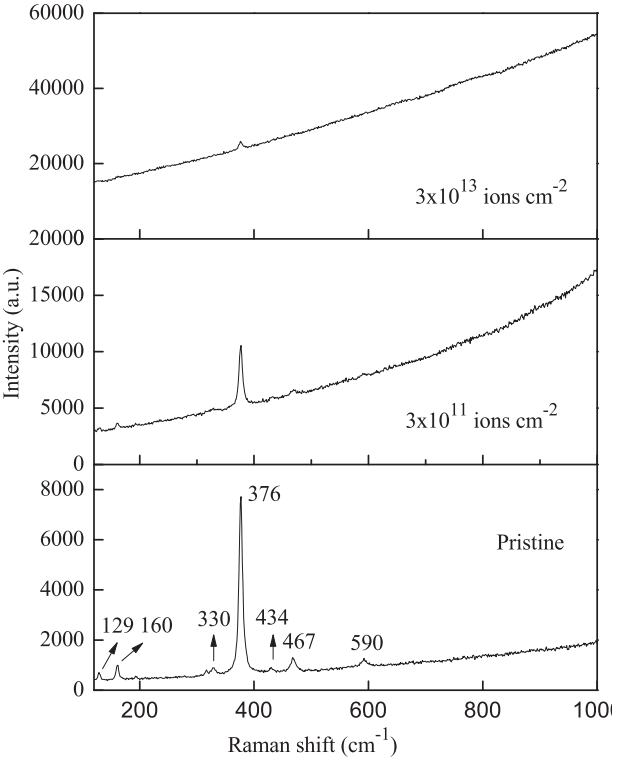

Figure 4. Raman spectra of pristine and SHI-irradiated Y_2O_3:Dy^{3+} nanophosphor.

high scattering intensity. This peak position is attributed to the Y–O vibration bond. SHI irradiation is expected to cause a decrease in all vibration modes intensity and full width half maxima of 376 cm^{-1} peak increases with an increase in ion fluence. At high fluence (3×10^{13} ions cm^{-2}), all Raman modes disappear except the 376 cm^{-1} mode (*22*). It indicates an increase in lattice damage in the samples and loss of crystalline nature.

3.4. Thermoluminescence

TL glow curves of pure and Dy^{3+}- (0.1–1.0 mol%) doped Y_2O_3 nanophosphor irradiated with 100 MeV Si^{8+} for fluence of 3×10^{11} ions cm^{-2} are shown in Figure 5. A well-resolved TL glow with peak at ~414 K and another one with peak at ~614 K are observed. Whereas in pure samples the lower temperature of the TL glow peak was observed at ~403 K besides the 600 K glow peak. The formation of traps at different depths corresponding to these TL glow peaks is the result of different penetrating levels of the SHI. The lower temperature peak (414 K) appears due to electrons being trapped at a shallow level, that is, F-center (*9*, *22*). The higher temperate peak at 614 K might be due to electrons activated from deep traps. The electrons captured by deep traps may go without getting retrapped at intermediate levels to the conduction band and recombine subsequently giving rise to the high-temperature glow peak. It is believed that energetic SHI creates oxygen vacancies and other structural lattice defects in the Y_2O_3:Dy^{3+} sample. The behaviors of the two peaks are different, because they arise from two different types of defect centers. Glow peak at 414 K is due to electrons trapped at the shallow level, that is, the F-center (*9*, *22*). The TL intensity at 414 K glow peak is found to increase with increasing Dy^{3+} molar concentration up to 0.6 mol% and thereafter decreases with a further increase in Dy^{3+} concentration as can be seen in the inset of Figure 5. This could be due to an increase in the number of luminescence centers with the Dy^{3+} content. Beyond 0.6 mol% the probability of energy transfer from traps to the luminescence centers decreases and hence the intensity. This effect is

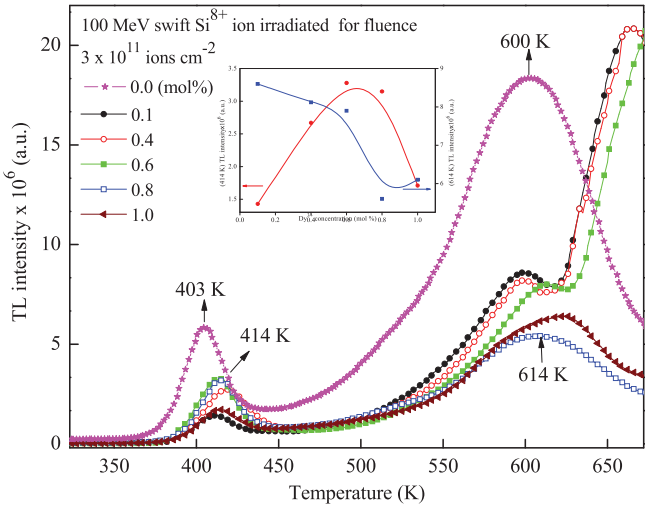

Figure 5. TL glow curves of 100 MeV swift Si^{8+} ions irradiated undoped and Dy^{3+} doped Y_2O_3. Inset: Variation of TL intensity and glow peak temperature as a function of dopant concentration.

known as concentration quenching (*17*). It indicates that Dy^{3+} creates more number of F-centers initially. During this process complex defect centers such as F_2-centers are formed resulting in decreased TL intensity corresponding to F-center. The high-temperate peak at 614 K might be due to deep level electron trap, that is, the F_2-center (*23*). The TL intensity at 614 K glow peak is found to decrease with increasing Dy^{3+} molar concentration. However, TL glow peak temperature at this peak is almost steady.

TL glow curves of 100 MeV swift Si^{8+} irradiated 0.6 mol% of Dy^{3+}-doped Y_2O_3 for various ion fluence in the range 3×10^{11}–3×10^{13} ions cm^{-2} are shown in Figure 6. It is observed that low temperature TL glow peaks (414 K) intensity decreases with increase in ion fluence while the higher temperature glow peak (614 K) intensity increases linearly up to 1×10^{12} ions cm^{-2} and then decreases with a further increase of ion fluence as shown in the inset of Figure 6. The saturation effect has been observed in the recorded ion fluence (Figure 3), and it is explained based on the track interaction model (*24*, *25*) and is quite suitable to explain the linear/sub linear/saturation response of nanophosphors in a long period of irradiation. According to this model, SHI could generate a track of length equal to the order of few 10s of nanometers.

At low fluences, electrons escaping their host tracks are intercepted by the nonradioactive competitive centers in the intermediate region between the tracks. The TL signal is proportional to the number of ion tracks. At high fluences the separation between neighboring ion tracks is reduced. Therefore, effective electrons escaping from tracks are more and more and recombine with luminescent centers, resulting in more TL signal. Furthermore, with an increase in ion fluence, the separation between the tracks is reduced resulting in overlapping of tracks causing reduction in TL signal hence resembling saturation. A further increase in ion fluence leads to reduction in the TL signal. In the present work, the saturation effect has not been observed due to low ion fluence (3×10^{11} ions cm^{-2}). SHI

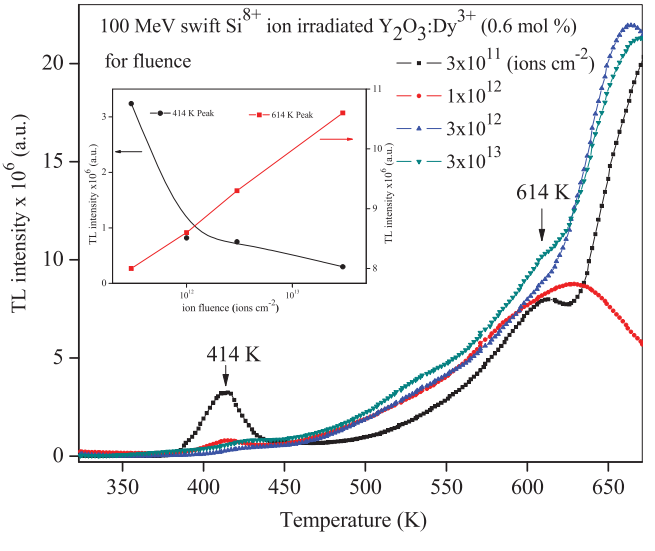

Figure 6. TL glow curves of SHI-irradiated Y_2O_3:Dy^{3+} nanophosphor for different fluences. Inset: Variation of TL intensity as a function of ion fluence.

induces more number of surface defects (oxygen vacancies) and they are responsible for ion tracks. However, the high-temperature glow peak (614 K) is found to increase linearly with an increase of ion fluence, but sub linear/saturation effect has not been observed.

The TL mechanism of the material may be explained based on the knowledge of kinetic parameters (trapping parameters), that is, activation energy (E), order of kinetics (b) and frequency factor (s) associated with the glow peaks. TL of Si^{8+} ion-irradiated Y_2O_3:Dy^{3+} nanophosphor exhibits broad TL glow due to overlapping of more than two glow peaks. The symmetry factor (μ_g) for this glow was estimated to be > 0.65. This value is greater than the allowed values for the first (0.42), second (0.52) and the general (values between 0.43 and 0.51) order of kinetics (*26*). Therefore, the above complex glow curve was deconvoluted using the GCD technique. The deconvoluted TL glow curves are obtained for the best fit of the theoretical curve with the experimental one. In the present work, the theoretical fit matches with experimental data for six deconvoluted peaks. The detailed GCD technique is discussed by Kitis et al. (*27*). They reported the TL glow curve equation of general order kinetics which is used for glow curve deconvolution

$$I(T) = I_m \cdot b^{b/(b-1)} \cdot \exp\left(\frac{E}{kT} \cdot \frac{T - T_m}{T_m}\right) \times \left[(b-1)\cdot(1-\Delta)\cdot\frac{T^2}{T_m^2} \times \exp\left(\frac{E}{kT}\cdot\frac{T-T_m}{T_m}\right) + Z_m\right]^{\cdot -b/(b-1)}, \quad (1)$$

where

$$\Delta = \frac{2kT}{E}; \Delta_m = \frac{2kT_m}{E}; Z_m = 1 + (b-1)\cdot\Delta_m,$$

where k is Boltzmann's constant (8.6×10^{-5} eV K^{-1}), β is the linear heating rate (5 K s^{-1}), I_m is the glow peak intensity and T_m is the glow peak temperature. The above equation can be inserted into an Excel spreadsheet. For the fitting procedure, one has to insert initial, arbitrary but meaningful values for the parameters I_m, T_m, E and b for each single glow peak. When the curve fitting procedure is completed, it gives the net values of I_m, T_m, E and b. In addition, the frequency factor and figure-of-merit (FOM) values are found (*28*). In the present work, theoretical fit matches with the experimental data for six deconvoluted peaks. The expression for the frequency factor and FOM are given by (*17*)

$$\frac{\beta E}{kT_m^2} = s\exp\frac{-E}{KT_m}[1 + (b-1)\Delta_m], \quad (2)$$

$$\text{FOM} = \frac{\sum|\text{TL}_{exp} - \text{TL}_{the}|}{\sum \text{TL}_{the}}. \quad (3)$$

Here, TL_{exp} and TL_{the} represent the TL intensity of experimental and theoretical glow curves, respectively. The deconvoluted TL curves of 100 MeV Si^{8+}-irradiated undoped and Dy-doped nanocrystalline Y_2O_3 for a fluence of 3×10^{11} ions cm^{-2} are shown in Figure 7 and 8. The FOM for the present curve fitting is found to be 1.80% and 1.94% for undoped and doped ion irradiation samples, respectively. This indicates a good agreement between theoretically generated and experimentally recorded TL glow curves. The deconvoluted experimental glow curves revealed different TL glows with peaks at 404, 433, 488, 538 and 606 K for undoped and peaks at 414, 422, 488, 533 and 606 K for ion-irradiated Dy-doped Y_2O_3. It is found that the above-deconvoluted glow obeys the general order kinetics.

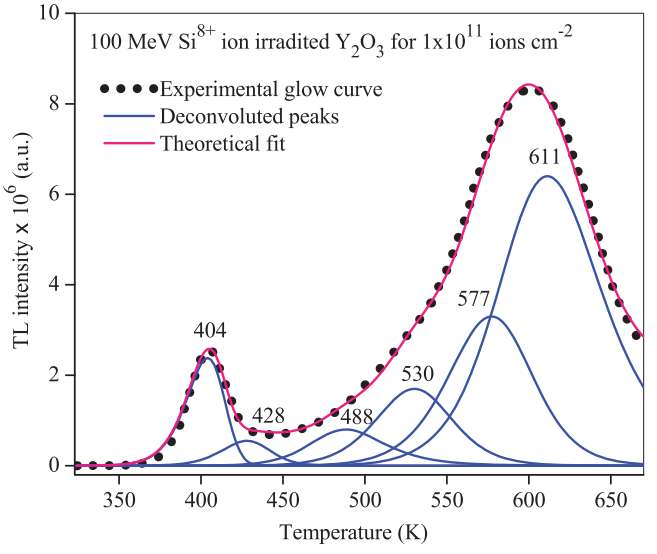

Figure 7. Deconvoluted TL glow curve of Y_2O_3 nanocrystal.

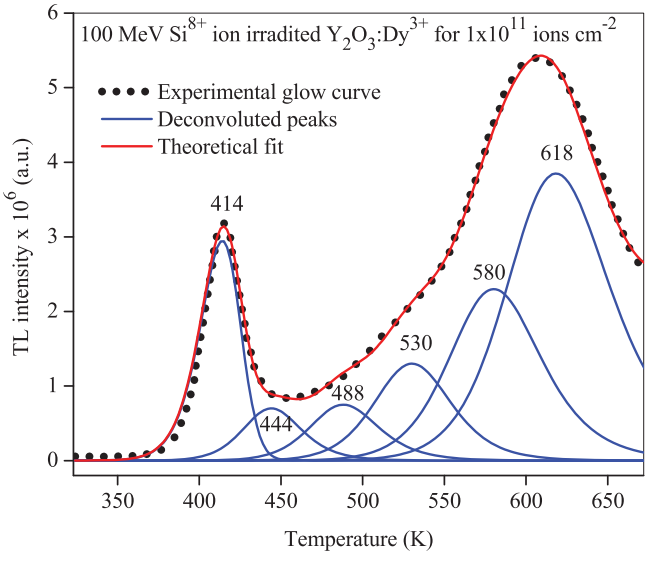

Figure 8. Deconvoluted TL glow curve of Y_2O_3:Dy^{3+} nanophosphor.

The activation energies are found to increase and the frequency factor decreases with an increase of TL glow peak temperature. The above trapping parameters are tabulated in Table 2. The activation energy of the Dy-doped Y_2O_3 sample shows a higher value when compared with that of the undoped sample. It is due to Dy^{3+} being incorporated in the Y^{3+} lattice modifying the band gap of the material, therefore the doped sample exhibited deeper traps of electron and holes center (*29*). The obtained activation energy and

Table 2. Trap parameters of TL glows of 100 MeV swift Si^{8+}-irradiated undoped and Dy^{3+}-doped Y_2O_3.

Samples	T_m (K)	B	E_{av} (eV)	s (s^{-1})	FOM (%)
Undoped (3×10^{11} ions cm^{-2})	404	1.15	1.25	1.73×10^{15}	
	433	1.8	1.30	5.21×10^{14}	
	488	2	1.33	1.66×10^{13}	1.80
	538	2	1.35	1.00×10^{12}	
	606	2	1.40	1.47×10^{10}	
Y_2O_3:Dy^{3+} (0.8 mol%) (3×10^{11} ions cm^{-2})	414	1.3	1.35	5.16×10^{16}	
	442	2	1.40	5.38×10^{15}	
	488	2	1.42	1.48×10^{14}	1.94
	533	2	1.44	7.11×10^{12}	
	606	2	1.47	3.95×10^{9}	

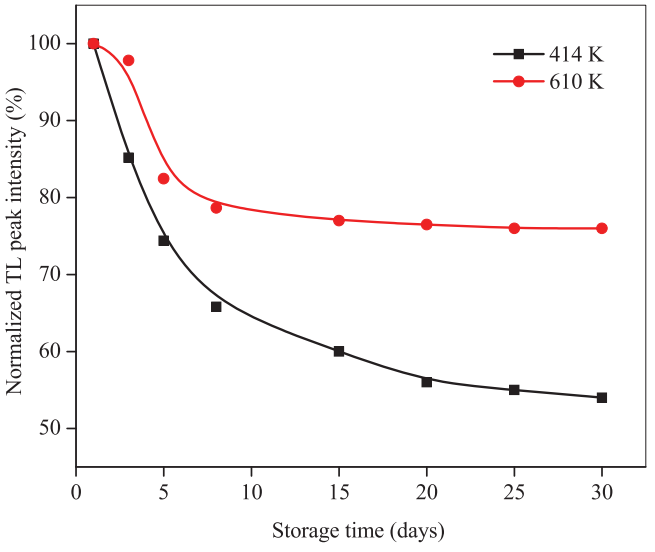

Figure 9. Effect of fading with storage time in Y_2O_3:Dy^{3+} nanophosphor.

frequency factor values are much closer to the standard dosimeter samples (*26*). Hence, this material might be used for high-energy space dosimeter applications.

3.4.1. TL fading effect

To study the effect of fading on TL glow curves of Y_2O_3:Dy^{3+}, samples were exposed for a test fluence of 5×10^{11} ions cm^{-2}. Figure 9 shows the plot of normalized TL intensity as a function of storage time after ion irradiation (*22*, *26*). Initially, the fading was very fast for the first eight days (33% and 21% for 414 and 614 K glow peaks, respectively) and later the fading became slow. It is found that there is 46% and 24% fading over a period of 30 days for 414 and 610 K glow peaks, respectively. These results conclude that high-temperature glow peak (614 K) is suitable for high-energy space dosimeter studies.

4. Conclusions

Combustion synthesized Dy^{3+}-doped Y_2O_3 exhibits cubic phase and an average crystallite size of $\sim$28 nm. The FE-SEM image shows well-separated spherical shape particles and the

average particle size is found to be in the range 40 nm. In the present studies, good TL efficiency was observed with an optimum Dy^{3+} dopant concentration of 0.6 mol%. The prominent high-temperature TL glow peak intensity increases linearly with ion fluence up to 3×10^{13} ions cm^{-2} in Dy^{3+}-doped Y_2O_3. It is observed that TL glow curves exhibit second-order kinetics since the retrapping of electron is high and the obtained activation energy and frequency factor are close to the standard dosimeter samples. The high-temperature glow peak (614 K) shows less fading over a period of 30 days. It is suggested that the present sample might be suitable for high-energy space dosimetry application.

Disclosure statement

No potential conflict of interest was reported by the authors.

Funding

The authors (NJS) express their sincere thanks to Inter University Accelerator Centre, New Delhi, India, for providing fellowship under UFR [No. 48303] scheme.

References

(1) Faucher, M.; Pannetier, J. *Acta Crystallogr. B.* **1980,** *36,* 3209.
(2) Singh, V.; Rai, V.K.; Ledoux-Rak, I.; Watanabe, S.; Gundu Rao, T.K.; Chubaci, J.F.D.; Badie, L.; Pelle, F.; Ivanova, S. *J. Phys. D: Appl. Phys.* **2009,** *42,* 065104.
(3) Jayasimhadri, M.; Ratanam, B.V.; Jang, K.; Lee, H.S.; Chen, B.; Yi, S.-S.; Jeong, J.-H.; Rama Moorthy, L. *J. Am. Ceram. Soc.* **2010,** *93,* 494.
(4) Vetrone, F.; Boyer, J.-C.; Capobianco, J.A.; Speghini, A.; Bettinelli, M. *Nanotechnology,* **2004,** *15,* 75.
(5) Gogotsi, Y. *Nanomaterials Hand Book;* CRC press, Taylor & Francis: New York, **2006**.
(6) Lakshminarasappa, B.N.; Jayaramaiah, J.R.; Nagabhushana, B.M. *Powder Tech.* **2012,** *217,* 7.
(7) Mimani, T.; Patil, K.C. *Mater. Phys. Mech.* **2001,** *4,* 134.
(8) Liu, J.; Hou, M.D.; Trautmann, C.; Neumann, R.; Müller, C.; Wang, Z.G.; Zhanga, Q.X.; Suna, Y.M.; Jina, Y.F.; Liuc, H.W.; Gao, H.J. *Nucl. Instrum. Methods B.* **2003,** *212,* 303.
(9) Salah, N.; Lochab, S.P.; Kanjilal, D.; Mehra, J.; Sahare, P.D.; Ranjan, R.; Rupasov, A.A.; Aleynikov, V.E. *J. Phys. D: Appl. Phys.* **2008,** *41,* 085408.
(10) Barth, W.; Dahl, L.; Glatz, J.; Groening, L.; Richter, S.; Yaramishev, S.: Proc. European Workshop on Beam Diagnostics and Instrumentation for Particle Accelerators, Mainz, Germany, 2003, 161.
(11) Strehl, P. Proc. 4th European Workshop on Beam Diagnostics and Instrumentation for Particle Accelerators, Chester, UK, 1999, 28.
(12) Lochab, S.P.; Salah, N.; Sahare, P.D.; Chauhan, R.S.; Ranjan, R. *Nucl. Instrum. Methods B.* **2007,** *254,* 231.
(13) Salah, N.; Sahare, P.D. *J. Phys. D. Appl. Phys.* **2006,** *39,* 2684.
(14) Necmeddin Yazici1, A.; Chen, R.; Solak, S.; Yegingil, Z. *J. Phys. D: Appl. Phys.* **2002,** *35,* 2526.
(15) Sanyal, B.; Natarajan, V.; Chawla, S.P.; Sharma, A. *Radiat. Meas.* **2010,** *45,* 899.
(16) Shivaramu, N.J.; Lakshminarasappa, B.N.; Nagabhushana, K.R.; Singh, F. *Radiat. Meas.* **2014,** *71,* 518.
(17) Shivaramu, N.J.; Lakshminarasappa, B.N.; Nagabhushana, K.R.; Singh, F. *J. Alloys Compd.* **2015,** *637,* 564.
(18) Szenes, G. *Phys. Rev. B.* **1999,** *60,* 3140.
(19) Guinebretière, R. X-ray Diffraction by Polycrystalline Materials, First published in France by Hermes Science, 2006.
(20) Mukherjee, S.; Sudarsan, V.; Sastry, P.U.; Patra, A.K.; Tyagi, A.K. *J. Lumin.* **2014,** *145,* 318.

(21) Ray, S.; León-Luis, S.F.; Manjón, F.J.; Mollar, M.A.; Gomis, Ó.; Rodríguez-Mendoza, U.R.; Agouram, S.; Muñoz, A.; Lavín, V. *Curr. Appl. Phys.* **2014,** *14,* 72.
(22) Shivaramu, N.J.; Lakshminarasappa, B.N.; Nagabhushana, K.R.; Singh, F. *Spectrochim. Acta A.* **2016,** *154,* 220.
(23) Lakshminarasappa, B.N.; Shivaramu, N.J.; Nagabhushana, K.R.; Singh, F. *Nucl. Instrum. Methods B.* **2014,** *329,* 40.
(24) Salah, N.; Sahare, P.D. *J. Phys. D Appl. Phys.* **2006,** *39,* 2684.
(25) Mahajna, S.; Horowitz, Y.S. *J. Phys. D: Appl. Phys.* **1997,** *30,* 2603.
(26) Mckeever, S.W.S. *Thermoluminescence of Solids*; Cambridge University Press: London, 1985.
(27) Kitis, G.; Gomez Ros, J.M.; Tuyn, J.W.N. *J. Phys. D. Appl. Phys.* **1998,** *31,* 2636.
(28) Afouxenidis, D.; Polymeris, G.S.; Tsirliganis, N.C.; Kitis, G. *Radiat. Protect Dosim.* **2012,** *149,* 363.
(29) Salah, N.; Habib, S.S.; Khan, Z.H.; Djouider, F. *Radiat. Phys. Chem.* **2011,** *80,* 923.